ELSEVIER

Journal of Alloys and Compounds 281 (1998) 137–145

Journal of ALLOYS AND COMPOUNDS

Crystal structure and chemistry of four new $RBa_4Cu_3O_{8.5+\delta}$ (R=Ho, Er, Tm and Yb) compounds

Y.T. Zhu, E.J. Peterson, P.S. Baldonado, J.Y. Coulter, D.E. Peterson*, F.M. Mueller

Mail Stop K763, Materials Science and Technology Division, Los Alamos National Laboratory, Los Alamos, NM 87545, USA

Received 17 April 1998; received in revised form 3 August 1998

Abstract

Four new $RBa_4Cu_3O_{8.5+\delta}$ (R143) compounds, where R=Ho, Er, Tm, and Yb, were synthesized from precursors Ho_2O_3, Er_2O_3, Tm_2O_3, Yb_2O_3, BaO_2, and CuO at 1000°C in an oxygen atmosphere. The oxygen stoichiometric value δ was found to be 0.50 for Ho143, 0.53 for Er143, 0.79 for Tm 143 and 1.01 for Yb143 by iodometric titration. Rietveld refinement of X-ray powder diffraction data showed that all the compounds belong to the space group $Pm\bar{3}$. The compounds have a cubic unit cell with lattice parameters of 8.09485±0.00007 Å for Ho143, 8.08236±0.00005 Å for Er143, 8.07670±0.00008 Å for Tm143, and 8.06198±0.00005 Å for Yb143. SQUID measurements indicated that none of the compounds was superconducting above 5 K. © 1998 Elsevier Science S.A. All rights reserved.

Keywords: Ho143; Er143; Tm143; Yb143; Rietveld refinement; Crystal structure; Space group; Cuprate

1. Introduction

In the search for possible new superconductors in the Y–Ba–Cu–O system, $YBa_4Cu_3O_{8.5+\delta}$ (Y143) was found by de Leeuw et al. [1,2] and Abbattista et al. [3,4], who refined the neutron and X-ray diffraction data of the Y143 phase, respectively, using the space group $Pm\bar{3}$. Y143 has a cubic structure, and would have some technological advantage if it was superconducting at temperatures comparable with high-temperature superconducting (HTS) materials [5]. To explore the 143 phases, we previously substituted Y with Sm, Eu, Gd and Dy to form $SmBa_4Cu_3O_{8.5+\delta}$ (Sm143) [6], $EuBa_4Cu_3O_{8.5+\delta}$ (Eu143) [7], $GdBa_4Cu_3O_{8.5+\delta}$ (Gd143) and $DyBa_4Cu_3O_{8.5+\delta}$ (Dy143) [8]. It was found from the Rietveld refinement of X-ray powder diffraction data that Sm143 and Gd143 belong to the space group $Pm\bar{3}$ [6,8], while Eu143 and Dy143 belong to the space $P\bar{2}3$ [7,8]. The two groups, $Pm\bar{3}$ and $P\bar{2}3$, are very similar. Their main difference is that, in $P\bar{2}3$, inversion symmetry is broken. During our further research in this area, four new 143 phases, $HoBa_4Cu_3O_{8.5+\delta}$ (Ho143), $ErBa_4Cu_3O_{8.5+\delta}$ (Er143), $TmBa_4Cu_3O_{8.5+\delta}$ (Tm143), $YbBa_4Cu_3O_{8.5+\delta}$ (Yb143), have been synthesized. In this paper, we report the synthesis, characterization and crystal chemistry of these four new 143 phases.

2. Experimental procedure

The R143 (R=Ho, Er, Tm, and Yb) compounds were synthesized in a similar way as Sm143, Eu143, Gd143 and Dy143 [6,7]. To prevent CO_2 contamination from air, all synthetic steps except sintering were performed inside a dry glove box. Ho_2O_3, Er_2O_3, Tm_2O_3, Yb_2O_3 BaO_2, and CuO were used as the precursor compounds, which were weighed to give an atomic ratio of R:Ba:Cu=1:4:3. The mixture of the powders was then thoroughly ground, pelleted, and fired at 950°C for 24 h in flowing oxygen. The resulting pellets were reground, repelleted, and then fired for the second time at 1000°C under flowing oxygen for 20 h. A slow cooling rate of 1°C/min. was used in the second sintering to maximize oxygen content in the final R143 compounds. A portion of the resulting pellets was ground for powder X-ray diffraction.

The sample was ground thoroughly using an agate mortar and pestle, after which silicon standard SRM 640b was blended in with the sample. This mixture was poured on top of a quartz zero background that had been lightly coated with silicone grease. Excess powder was then

*Corresponding author.

0925-8388/98/$ – see front matter © 1998 Elsevier Science S.A. All rights reserved.
PII: S0925-8388(98)00798-1

removed by softly tapping the sample holder on edge, leaving a thin layer of powder particles coating the quartz plate. Powder X-ray diffraction data were collected using a Scintag XDS2000 θ–θ powder diffractometer equipped with a graphite monochromator in conjunction with a scintillation detector. Cu Kα ($K\alpha_1$=1.54056 Å, $K\alpha_2$= 1.54439 Å) radiation was used to collect data. The sample was rotated during data collection. Three data sets were collected; (1) a continuous scan from 2 to 70° 2θ with a chopper size of 0.03°, (2) a step scan from 20 to 90° 2θ with a step size of 0.02°, and a count time of 7 s, and (3) a step scan from 70 to 140° 2θ with a step of 0.04° and a count time of 14 s. The first scan was done to verify phase purity, while the second and third scans were employed as data bases for the Rietveld analysis.

Iodometric titration was performed using a Mettler DL40RC titrator under inert atmosphere to determine oxygen content in the samples. It is well known that the solution may absorb oxygen from air during the titration, resulting in error of the experimental data. This error was eliminated by doing the titration under He. A superconducting quantum interference device (SQUID) magnetometer (Quantum Design) was used to measure the susceptibility of the samples. A small piece of sample pellet was measured over a temperature range of 5–120 K, and under an applied field of 10 Oe. All samples were zero-field cooled before the susceptibility measurements.

3. Rietveld refinement and discussion

The powder X-ray step scan data sets were analyzed simultaneously by the Rietveld method using the computer program GSAS [9]. A pseudo-Voigt function was used to fit the Bragg diffraction peaks and a cosine Fourier series with six coefficients was used to model the background. To determine which space group fits the X-ray data better, both $Pm\bar{3}$ and $P2\bar{3}$ space groups were used in the refinement. The two space groups have similar atomic arrangement in their unit cell (Fig. 1). However, $P2\bar{3}$ has a lower order and treats the Ba atoms, which are equivalent in $Pm\bar{3}$, as two distinct sets (B1 and B2). During the Rietveld refinement, $P2\bar{3}$ allows the B1 and B2 positions to be refined independently. The $Pm\bar{3}$ space group is essentially a special case of the $P2\bar{3}$ space group. If a compound belongs to the space group $Pm\bar{3}$, it must also belong to the space group P23, and the Rietveld refinement using both space groups should yield the same results. On the other hand, if a compound belongs to the space group $P2\bar{3}$, but not $Pm\bar{3}$, the Rietveld refinement using the space groups $P2\bar{3}$ will yield different results from using the space group $Pm\bar{3}$.

The δ values were determined by iodometric titration as 0.50 for Ho143, 0.53 for Er143, 0.79 for Tm 143 and 1.01 for Yb143. Initial values for atomic positions were assumed to be the same as $YBa_4Cu_3O_{8.5+\delta}$ [2] when $Pm\bar{3}$ space group was used and $EuBa_4Cu_3O_{8.5+\delta}$ [7] when $P2\bar{3}$ space group was used. The silicon lattice parameter was set at its known value of 5.43094 Å and the sample displacement was allowed to vary. The lattice parameters for R143 phases were refined. The L_x and L_y profile parameters (for the particle size and strain effect) were refined and showed essentially no size and very little strain effects for all compounds, when compared to previously refined values for the LaB_6 profile standard SRM 660.

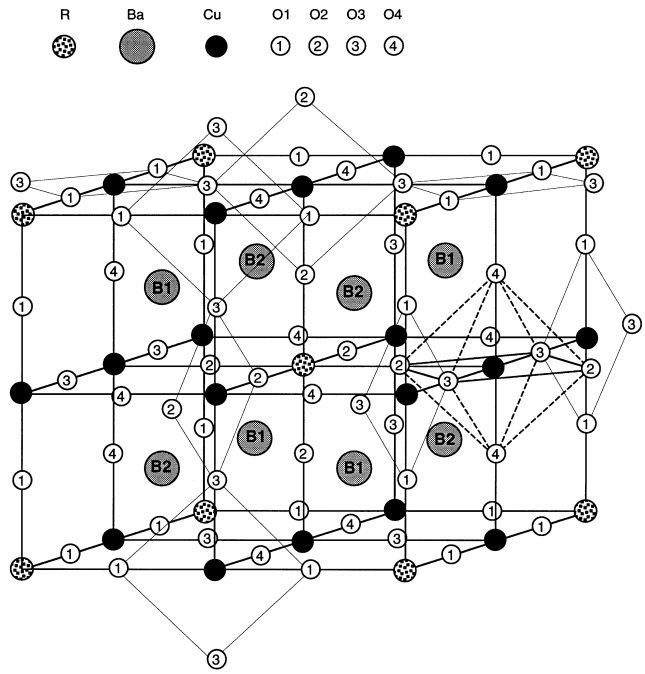

Fig. 1. The unit cell (two formula) of R143.

For both the space groups, the positions of Ba atoms, and O1 and O2 sites were refined, except for Yb143 in which case the refinement of Ba positions failed when using the $P2\bar{3}$ space group. The individual isotropic temperature factors for each type of atom was also refined (i.e. $U_{\text{isotropic}}$ was constrained to be the same value for all atoms of the same type, but was allowed to vary independently from the $U_{\text{isotropic}}$ of other types of atoms).

To automatically refine the oxygen occupancies on the O3 and O4 sites, we found it necessary to first determine their approximate values by manually checking the goodness of fit, χ^2, as a function of O3 and O4 site occupancy. A smaller χ^2 value means a better fit. In addition, the space group can also be determined from the χ^2 versus oxygen occupancy curve [7,8]. For example, the space group $P2\bar{3}$ yielded significantly lower χ^2 values over the entire range of O occupancies in Eu143 [7] than $Pm\bar{3}$, which indicates that $P2\bar{3}$ fits the X-ray data better. It can be calculated [10] from the oxygen content that the sum of the occupancies in O3 and O4 sites should equal 1.00 for Ho143, 1.01 for Er143, 1.10 for Tm143 and 1.17 for Yb143, where the occupancy is defined as the fraction of O3 or O4 sites occupied by the oxygen atoms. The χ^2

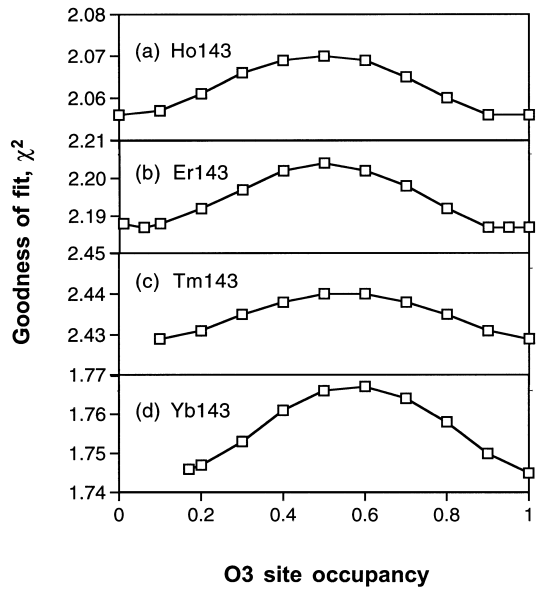

Fig. 2. The goodness of fit, χ^2, for the space group $Pm\bar{3}$ as a function of O3 and O4 site occupancy for: (a) Ho143, (b) Er143, (c) Tm143 and (d) Yb143.

Table 1
The statistics of the X-ray profile fittings for the R143 phases

Statistics	Ho143	Er143	Tm143	Yb143
χ^2	2.056	2.187	2.429	1.745
wRp	0.1082	0.1034	0.1323	0.1006
Rp	0.0777	0.0753	0.0973	0.0873
U_{iso} (R)	0.00473	0.00585	0.00186	0.00665
U_{iso} (Ba)	0. 00473	0.00851	0.00605	0.00937
U_{iso} (Cu)	0. 00473	0.00798	0.00661	0.00982
U_{iso} (O)	0.00482	0.00116	0.00925	0.01082
L_x	2.026	2.912	3.133	1.722
L_y	11.479	8.303	12.015	9.444

χ^2 is the goodness of fit, wRp is weighed residual, Rp is residual, U_{iso} is the isotropic temperature factor. L_x is the particle size broadening, and L_y is the strain broadening. See Ref. [9] for more details on definition.

Table 2
The atomic positions and site occupancies obtained by Rietveld refinement for: (a) Ho143, (b) Er143, (c) Tm143 and (d) Yb143

Position	x	y	z	n	
(a) Ho143					
Ho1	(1a)	0	0	0	1
Ho2	(1b)	0.5	0.5	0.5	1
Ba	(8i)	0.24887	0.24887	0.24887	8
Cu1	(3d)	0.5	0	0	4
Cu2	(3c)	0	0.5	0.5	4
O1	(6e)	0.26791	0	0	6
O2	(6h)	0.23239	0.5	0.5	6
O3	(6f)	0.25124	0	0.5	0.04 or 5.72
O4	(6g)	0.24	0.5	0	5.96 or 0.28
(b) Er143					
Er1	(1a)	0	0	0	1
Er2	(1b)	0.5	0.5	0.5	1
Ba	(8i)	0.25075	0. 25075	0. 25075	8
Cu1	(3d)	0.5	0	0	4
Cu2	(3c)	0	0.5	0.5	4
O1	(6e)	0.27778	0	0	6
O2	(6h)	0.22962	0.5	0.5	6
O3	(6f)	0.25124	0	0.5	0.36 or 5.70
O4	(6g)	0.24	0.5	0	5.70 or 0.36
(c) Tm143					
Tm1	(1a)	0	0	0	1
Tm2	(1b)	0.5	0.5	0.5	1
Ba	(8i)	0.25031	0. 25031	0. 25031	8
Cu1	(3d)	0.5	0	0	4
Cu2	(3c)	0	0.5	0.5	4
O1	(6e)	0.28114	0	0	6
O2	(6h)	0.23415	0.5	0.5	6
O3	(6f)	0.25124	0	0.5	0.6 or 6
O4	(6g)	0.24	0.5	0	6 or 0.6
(d) Yb143					
Yb1	(1a)	0	0	0	1
Yb2	(1b)	0.5	0.5	0.5	1
Ba	(8i)	0.25040	0. 25040	0. 25040	8
Cu1	(3d)	0.5	0	0	4
Cu2	(3c)	0	0.5	0.5	4
O1	(6e)	0.2729	0	0	6
O2	(6h)	0.22838	0.5	0.5	6
O3	(6f)	0.25124	0	0.5	1.02 or 6
O4	(6g)	0.24	0.5	0	6 or 1.02

The positions of O3 and O4 sites are from de Leeuw et al. [2]. n is the number of atoms per unit cell occupying each position.

Table 3
Strains in the R–O1–Cu–O1–R and Cu–O3–Cu–O3–Cu bonds

R143	Lattice constant (Å)	Occupancy		Average r (Cu^{2+}) (Å)	R–O1–Cu–O1–R		Cu–O3–Cu–O3–Cu	
		O3 (%)	O4 (%)		Length (Å)	Strain (%)	Length (Å)	Strain (%)
Ho143	8.09458	99.3	0.7	0.5711	8.522	−5.28	7.884	2.60
		50	50	0.65	8.68	−7.23	8.200	−1.30
Er143	8.08236	95	6	0.5796	8.5192	−5.40	7.9184	2.03
		50.5	50.5	0.6508	8.6616	−7.17	8.2032	−1.50
Tm143	8.07670	100	10	0.586	8.512	−5.39	7.944	1.64
		55	55	0.658	8.656	−7.17	8.232	−1.92
Yb143	8.06198	100	17	0.5972	8.5114	−5.61	7.9888	0.91
		58.5	58.5	0.6636	8.6472	−7.23	8.2544	−2.39

Nonuniform oxygen distribution in the O3 and O4 sites results in compressive strain (negative value) in R–O1–Cu–O1–R bonds and tensile strain in Cu–O3–Cu–O3–Cu bonds, while uniform oxygen distribution results in compressive strain in both types of bonds.

obtained from the manual refinement are plotted in Fig. 2 as a function of O3 site occupancy. For all R143 phases except Yb143, space group Pm3 and P23 yield identical χ^2 values for the full range of O3 occupancy. For Yb143, only Pm3 space group allows a convergent refinement of Ba atomic position. Since lowering the crystal symmetry from Pm3 to P23 does not improve the goodness of fit, χ^2, for any of these compounds, we have assumed that is Pm3 the correct space group for all compounds [8].

The statistics of the X-ray profile fittings for all compounds are listed in Table 1. The lattice parameter of the unit cell did not vary much with varying oxygen occupancy on the O3 and O4 sites, and was refined as 8.09485±0.00007 Å for Ho143 and 8.08236±0.00005 Å for Er143, 8.07670±0.00008 Å for Tm143, and 8.06198±0.00005 Å for Yb143. The positions of both Ba atom and O1 and O2 sites have been refined. Listed in Table 2 are the atomic positions and the number of atoms occupying each position, *n*, for all four R143 compounds. For Ho143 (Table 2), the occupancies of O3 and O4 sites are 0.7 and 99.3%, respectively, or 95.3 and 4.7%, respectively. For Er143 (Table 2), the occupancies of O3 and O4 sites are 6 and 95%, respectively, or 95 and 6%, respectively. The O3 and O4 sites in Tm143 are occupied by 10 and 100%, respectively, or 100 and 10%, respectively (Table 2). The O3 and O4 sites in Yb143 are occupied by 17 and 100%, respectively, or 100 and 17%, respectively (Table 2). Therefore, the O3 and O4 sites are not occupied uniformly in any of the four compounds.

The oxygen distributions in these four R143 compounds are similar to that in Y143 [10]. The nonuniform distribution has been attributed to the Cu^{2+} radius variation associated with different coordination and the stress balance in different cation–oxygen bonds [10]. Fig. 1 represents the crystal lattice of R143 when O4 sites are almost empty and O3 sites are almost fully occupied. It can be seen that most of the Cu^{2+} ions are coordinated by four O^{2-} ions in a square arrangement. An occupied O4 site can effectively create two Cu^{2+} ions coordinated by five O^{2-} ions (which is equivalent to one Cu^{2+} ion coordinated by six O^{2-} ions). The Cu^{2+} ion has an ionic radius of 0.57 (for four-fold square coordination, and 0.73 (for six-fold octahedral coordination [11]. Therefore, decreasing the O4 site occupancy will lead to decrease in the average ionic radius of Cu^{2+}, and subsequently a decrease in the overall lattice parameter.

The lengths of different cation–oxygen bonds in the crystal structure usually do not match each other, causing stresses in these bonds [12,13]. These stresses need to balance each other. The nonuniform distribution of oxygen in the O3 and O4 sites is a natural way to adjust the lattice parameter so as to balance these stresses. To prove this hypothesis, we need to analyze the stresses (strains) in these bonds. Fig. 1 shows that the R–O1–Cu–O1–R bonds and the Cu–O3–Cu–O3–Cu bonds are parallel to each other. Stresses exist in these two types of bonds since they

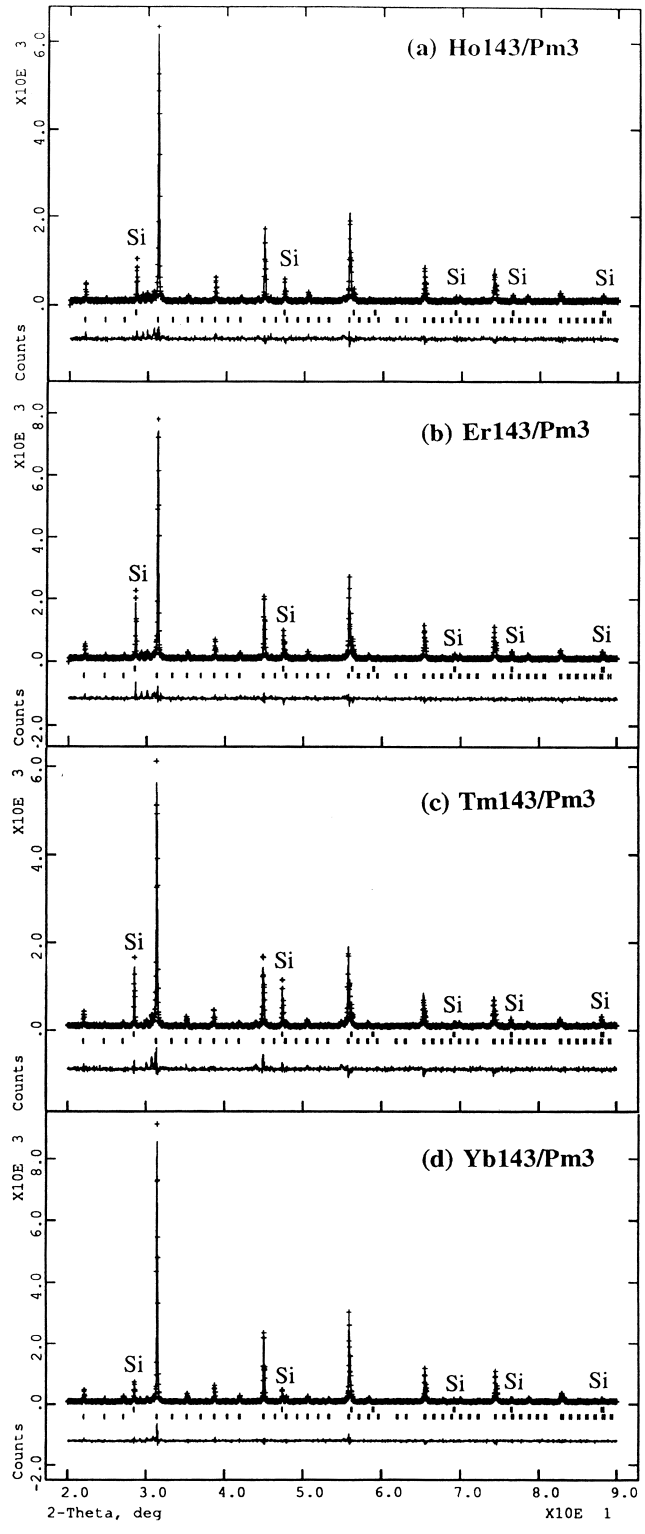

Fig. 3. X-ray powder diffraction profiles for: (a) Ho143, (b) Er143, (c) Tm143 and (d) Yb143. The diffraction peaks marked as Si are from silicon standard. In the top part of the figure, the solid line represents the fit to the data as calculated by the Rietveld refinement with parameters listed in Table 2, while the location of + signs represent the observed intensity. The lower part represents the difference between the observed and the calculated profile.

Table 4
X-ray powder diffraction data of the R143 compounds

2θ	d (Å)	I/I_{100}0bs (integrated)	I/I_{100}Cal (integrated)	I/I_{100}0bs (peak height)	hkl
Ho143					
10.92	8.0948	—	—	0.2	100
15.47	5.7239	—	—	3.4	110
18.97	4.6736	—	—	0.4	111
21.94	4.0474	5.7	3.2	6.3	200
24.57	3.6201	0.4	0.7	0.2	201
26.96	3.3047	0.1	0.2	0.1	211
31.23	2.8620	100.0	100.0	100.0	220
35.03	2.5598	1.1	1.4	0.6	310
38.49	2.3368	8.9	7.0	4.6	222
40.13	2.2451	0.1	0.2	0.3	302
41.72	2.1634	1.0	1.0	0.3	321
44.75	2.0237	26.6	29.2	26.5	400
47.62	1.9080	0.8	1.0	0.2	330, 411
50.37	1.8101	3.8	2.2	1.8	402
53.02	1.7258	0.6	0.5	—	332
55.57	1.6523	42.1	43.1	30.7	422
56.82	1.6190	0.3	0.0	0.1	403, 500
58.05	1.5875	0.5	0.7	—	431, 501
61.65	1.5032	0.4	0.1	—	423, 502
62.83	1.4779	0.2	0.2	—	521
65.13	1.4310	17.8	19.5	12.3	440
67.40	1.3883	0.3	0.4	0.6	433, 503
69.63	1.3491	2.0	1.9	1.3	600, 442
71.83	1.3132	0.2	0.2	0.1	611, 523
74.00	1.2799	17.9	19.9	10.8	620
76.15	1.2491	0.2	0.2	—	541
78.28	1.2203	3.0	3.4	1.9	622
80.39	1.1935	0.6	0.4	0.2	631
82.49	1.1684	6.2	6.8	2.9	444
84.58	1.1448	0.3	0.4	—	550, 543, 710
86.66	1.1226	1.2	1.0	0.4	640
88.74	1.1016	0.4	0.4	—	712, 552, 633
90.81	1.0817	67.0	28.2	10.5	624
92.89	1.0629	0.4	0.2	0.3	730
99.15	1.0119	3.1	3.3	1.6	800
101.26	0.99641	0.2	0.3	—	811, 554, 741
103.38	0.98164	1.6	3.1	0.8	820, 644
104.45	0.97451	0.2	0.1	—	742, 812
105.53	0.96752	0.2	0.2	—	635
107.69	0.95399	14.0	13.7	4.4	822,660
109.88	0.94101	0.3	0.4	0.1	813, 743, 750
112.11	0.92854	2.1	1.7	0.8	662
114.37	0.91656	0.2	0.1	0.3	725
116.67	0.90503	11.9	11.3	3.5	804
119.01	0.89393	0.5	0.3	0.4	910,833
121.41	0.88322	2.0	2.1	0.8	842
Er143					
10.94	8.0824	—	—	0.3	100
15.49	5.7151	—	—	4.6	110
19.00	4.6663	—	—	0.3	111
21.98	4.0412	4.5	2.9	0.7	200
24.61	3.6145	0.2	0.6	0.1	210
27.00	3.2996	0.9	1.0	0.7	211
31.28	2.8575	100.0	100.0	100.0	220
35.08	2.5559	2.1	2.4	0.4	310
38.56	2.3332	7.3	6.6	7.3	222
40.20	2.2416	0.2	0.1	0.2	302
41.78	2.1601	2.2	1.8	0.6	321
44.82	2.0206	27.3	28.9	27.5	400
47.70	1.9050	1.4	1.4	0.4	330, 411
50.46	1.8073	4.2	2.9	2.5	402
51.79	1.7637	0.1	0.1	—	412

Table 4. Continued

2θ	d (Å)	I/I_{100}0bs (integrated)	I/I_{100}Cal (integrated)	I/I_{100}0bs (peak height)	hkl
53.11	1.7232	0.9	0.7	0.1	332
55.67	1.6498	41.2	41.6	32.9	422
58.15	1.5851	1.6	1.5	0.6	510, 413
61.76	1.5009	0.2	0.1	—	432, 502
62.93	1.4756	0.2	0.2	—	512
65.25	1.4288	18.1	18.9	13.9	440
67.52	1.3861	0.9	0.8	0.1	503, 433
69.76	1.3471	1.4	1.8	0.5	442, 600
71.96	1.3111	0.2	0.3	0.3	523, 611
74.14	1.2779	17.8	19.1	12.4	602
76.29	1.2471	0.4	0.3	0.2	541
78.42	1.2185	2.6	2.7	1.4	622
80.54	1.1917	0.9	0.5	0.1	631
82.64	1.1666	5.8	6.4	3.2	444
84.74	1.1430	0.6	0.6	0.1	534, 710, 550
86.83	1.1208	0.9	0.6	0.1	640
88.91	1.0999	0.5	0.5	—	712, 552, 633
90.99	1.0800	21.5	22.9	12.5	642
93.07	1.0613	0.6	0.4	0.2	703
97.25	1.0265	0.3	0.4	0.4	615, 732
99.36	1.0103	2.6	3.1	1.8	800
101.47	0.99487	0.2	0.3	—	811, 554, 741
103.61	0.98013	0.9	1.3	0.7	820, 644
105.76	0.96603	0.3	0.2	—	635
107.94	0.95251	13.2	12.7	6.0	822, 660
110.14	0.93955	0.7	0.7	0.5	734, 831, 750
112.37	0.92711	1.3	1.6	0.8	662
114.64	0.91515	0.3	0.2	—	752
116.95	0.90363	11.4	10.6	4.7	840
Tm143					
10.945	8.0767	—	—	0.1	100
15.503	5.7111	—	—	5.9	110
19.016	4.6631	—	—	0.3	111
21.992	4.0384	4.2	2.4	1.3	200
24.626	3.6120	0.5	0.6	0.1	210
27.019	3.2973	1.3	1.5	1.1	211
31.299	2.8555	100.0	100.0	100.0	220
35.106	2.5541	2.5	2.7	3.8	310
38.583	2.3315	6.2	6.3	6.5	222
41.813	2.1586	1.3	1.7	1.8	321
44.851	2.0192	29.4	29.3	29.8	400
47.735	1.9037	1.7	1.7	1.1	330,411
50.493	1.8060	2.3	2.0	2.3	402
51.831	1.7625	0.2	0.1	0.2	412
53.145	1.7722	0.7	0.8	0.3	332
55.708	1.6487	39.1	42.6	28.6	422
56.960	1.6153	0.3	0.0	—	500,403
58.195	1.5840	1.7	1.8	0.9	510,413
62.982	1.4746	0.2	0.3	0.2	512
65.299	1.4278	16.9	19.2	10.0	440
67.573	1.3851	0.8	0.9	0.5	530, 433
69.811	1.3461	1.6	1.2	0.7	442, 600
72.017	1.3102	0.8	0.7	0.3	523, 611
74.195	1.2770	17.1	20.1	11.2	602
76.351	1.2463	0.5	0.4	0.2	541
78.487	1.2176	2.2	2.5	0.7	622
80.607	1.1908	0.9	0.6	—	631
82.714	1.1658	5.4	6.6	2.2	444
84.811	1.1422	1.1	0.9	—	534, 710, 550
86.901	1.1200	0.9	0.6	0.2	640
88.987	1.0991	0.9	0.8	0.1	712, 552, 633
91.072	1.0793	21.7	24.2	9.1	642
97.346	1.0257	0.6	0.7	0.5	732, 651

Table 4. Continued

2θ	d (Å)	I/I_{100}0bs (integrated)	I/I_{100}Cal (integrated)	I/I_{100}0bs (peak height)	hkl
99.452	1.0096	3.3	3.3	1.5	800
101.57	0.99417	0.4	0.5	0.3	741, 554, 811
103.71	0.97944	1.3	1.6	0.6	820, 644
105.87	0.96535	0.7	0.4	—	635
108.04	0.95185	14.2	13.9	5.2	822, 660
110.25	0.93890	0.8	0.9	0.2	734, 831, 750
112.49	0.92646	1.0	1.62	0.3	662
114.76	0.91451	0.3	0.3	0.2	725
117.08	0.90300	11.3	11.0	3.5	840
119.45	0.89192	0.1	0.1	—	833, 901
124.36	0.87093	0.2	0.4	—	761, 655, 921
126.93	0.86098	19.7	14.1	4.8	664
129.58	0.85136	0.5	0.6	0.3	745, 851, 903
Yb143					
10.97	8.0620	—	—	0.2	100
15.53	5.7007	—	—	7.3	110
19.05	4.6546	—	—	0.2	111
22.03	4.0310	3.7	2.4	4.3	200
24.67	3.6054	0.3	0.5	1.1	210
27.07	3.2913	1.6	1.8	2.21	211
31.36	2.8503	100.0	100.0	100.0	220
35.17	2.5494	2.8	2.9	3.6	310
38.66	2.3273	6.4	6.2	6.0	222
41.89	2.1546	2.4	2.3	2.0	321
44.94	2.0155	27.2	29.0	25.1	400
47.83	1.9002	1.6	1.7	1.5	330, 411
50.59	1.8027	2.0	1.9	1.8	402
51.93	1.7593	0.2	0.1	0.2	412
53.25	1.7188	0.8	0.8	1.1	332
55.82	1.6456	41.1	41.7	30.1	422
58.31	1.5811	1.8	1.8	1.5	510, 413
61.93	1.4971	0.2	0.1	0.2	432, 502
63.11	1.4719	1.1	0.3	0.3	512
65.43	1.4252	17.1	18.6	11.4	440
67.71	1.3826	0.8	0.9	0.4	503, 433
69.96	1.3437	1.2	1.4	0.9	442, 600
72.17	1.3078	0.5	0.6	0.6	523, 611
74.35	1.2747	17.2	19.0	10.9	602
76.52	1.2440	0.4	0.4	0.4	541
78.66	1.2154	1.9	2.5	0.3	622
80.79	1.1887	1.0	0.6	0.2	631
82.90	1.1637	5.7	6.3	2.9	444
85.00	1.1401	0.9	0.8	0.3	534, 710, 550
87.10	1.1180	0.8	0.6	0.3	640
89.19	1.0971	0.7	0.8	0.3	552, 712, 633
91.29	1.0773	20.8	22.6	10.2	624
93.38	1.0586	0.5	0.3	0.1	730
97.58	1.0239	0.5	0.6	0.2	723, 651
99.70	1.0078	3.5	1.7	1.3	800
101.83	0.9924	0.5	0.6	0.2	554, 714, 811
103.98	0.9777	1.3	1.1	0.5	644, 820
108.33	0.9501	13.0	12.6	4.9	660, 822
110.55	0.9372	1.0	1.0	0.5	750, 743, 831
112.80	0.9248	0.9	1.43	0.6	662
115.09	0.9128	0.3	0.3	—	725
117.43	0.9014	10.7	10.0	3.9	804
119.81	0.8903	0.3	0.3	—	901, 833
122.25	0.8796	1.3	1.2	0.6	824
124.76	0.8694	0.7	0.6	0.2	912, 761, 655
127.35	0.8594	9.8	8.1	2.8	664

do not have the same length. The O^{2-} ion is coordinated by six cations and has an ionic radius of 1.4 Å. The ionic radius of the rare earth ions (coordinated by six O^{2-}) are: Ho^{3+}=0.89 Å, Er^{3+}=0.88 Å, Tm^{3+}=0.87 Å, Yb^{3+}=0.86 Å. Assuming that the O^{2-} ions preferably occupy the O3 sites, the average radius of Cu^{2+} can be interpolated according to the occupancy of the O4 sites, under the approximation that each occupied O4 site create a Cu^{2+} ion with a six-fold coordination. The calculated strains in R–O1–Cu–O1–R and the Cu–O3–Cu–O3–Cu bonds are listed in Table 3. For all of the four compounds, the R–O1–Cu–O1–R bonds are in compressive strain and the Cu–O3–Cu–O3–Cu bonds are in tensile strain, if the oxygen occupies the O3 and O4 sites nonuniformly as determined by the Rietveld refinements. Therefore, the compressive stress in the R–O1–Cu–O1–R bonds will balance the tensile stress in the Cu–O3–Cu–O3–Cu bonds. However, if the oxygen uniformly occupies the O3 and O4 sites, both the R–O1–Cu–O1–R and the Cu–O3–Cu–O3–Cu bonds will be in compression, which is unlikely. These internal stresses in different bonds need to balance and partially cancel each other. It takes a certain occupancy of the O4 sites to yield an average Cu^{2+} radius that balances the stresses in all the bonds, which explains why the O3 and O4 sites are not evenly occupied by oxygen atoms. Note that the above analysis is only qualitative and does not include the stress in the Ba–O bonds. Nevertheless, it does demonstrate that the nonuniform distribution of oxygen in the O3 and O4 sites are due to stresses in different cation–oxygen bonds.

Fig. 3 shows the X-ray powder diffraction profiles for: (a) Ho143, (b) Er143, (c) Tm143 and (d) Yb143. In the top part of each figure, the solid line represents the fit to the data as calculated with parameters listed in Table 2, while the location of + signs represent the observed intensity. The lower part represents the difference between the observed and the calculated profile. The calculated X-ray diffraction profile agrees with the experimental data very well.

Table 4 lists the *d* spacing of crystal planes, the observed and the calculated integrated relative intensities of X-ray deflection peaks (obtained from GSAS) and peak height relative intensities (obtained from profile fitting of peaks using the Scintag DMS software with a Pearson VII profile function) for the four R143 compounds.

A superconducting quantum interference device (SQUID) magnetometer (Quantum Design) was used to check the superconductivity of the as-synthesized R143 compounds. The magnetization of a sample pellet was measured over a temperature range of 5–120 K, and under an applied field of 10 Oe. The temperature dependence of the specific magnetization and its inverse values are shown in Fig. 4. No diamagnetic behavior was found for any of these compounds over the temperature range of 5–150 K. So we believe that none of them are superconducting in the range of our measurements. As it can be seen the magnetization follows mostly a Curie–Weiss behavior, with a

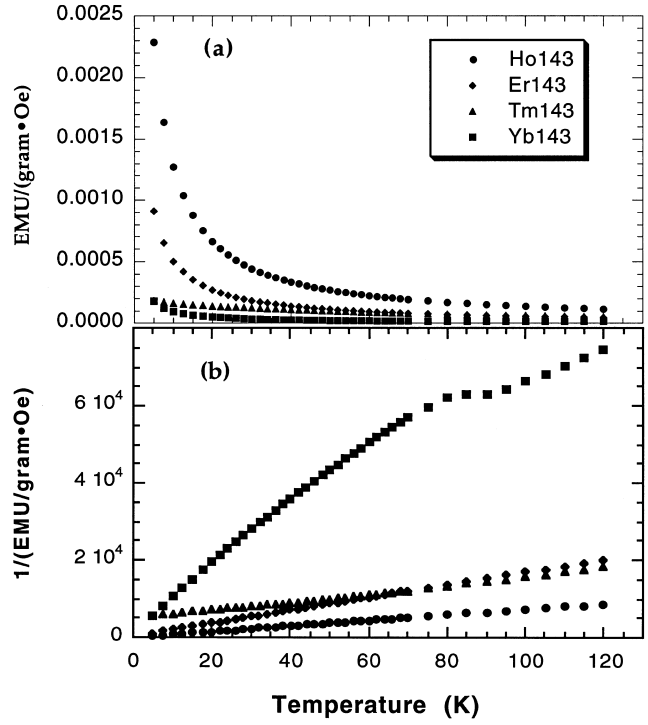

Fig. 4. Temperature dependence of (a) the specific magnetization and (b) its inverse values for the four R143 compounds.

Curie temperature of approximately 0 K. This is similar to measurements carried out in $RBa_2Cu_3O_7$ (R=rare earth) compounds [14]. Superposed on this general behavior is another magnetic phenomena which causes the magnetization to exhibit a local cusp. The cusp appears in all four of these compounds at about 75–90 K. We believe that these two phenomena are due to separate ordering of copper d-electron and rare-earth f-electron magnetic moments on their two respective sub-lattices. Similar models have been used to interpret magnetic behaviors in high temperature superconducting (HTS) materials [15].

4. Conclusions

We have successfully synthesized four new R143 compounds $HoBa_4Cu_3O_{8.5+\delta}$ and $ErBa_4Cu_3O_{8.5+\delta}$, $TmBa_4Cu_3O_{8.5+\delta}$ and $YbBa_4Cu_3O_{8.5+\delta}$. Rietveld refinement of X-ray data indicates that all compounds belongs to space group $Pm\bar{3}$. All compounds has a cubic structure and their lattice parameters have been refined as 8.09485±0.00007 Å for Ho143, 8.08236±0.00005 Å for Er143, 8.07670±0.00008 Å for Tm143, and 8.06198±0.00005 Å for Yb143. Oxygen distributions in the O3 and O4 sites are found to be nonuniform, which was caused by the internal stresses in different cation–oxygen bonds. SQUID measurements have indicated that all these compounds were not superconducting above 5 K.

Acknowledgements

Support was provided by the Superconductivity Technology Center (STC) of Los Alamos National Laboratory through the US DOE Office of Energy Management. This work was performed at the Los Alamos National Laboratory under the auspices of the US Department of Energy (contract W-7405-ENG-36).

References

[1] D.M. de Leeuw, C.A.H.A. Mutsaers, C. Langereis, H.C.A. Smoorenburg, P.J. Rommers, Physica C 152 (1988) 39.
[2] D.M. de Leeuw, C.A.H.A. Mutsaers, R.A. Streetman, E. Frikkee, H.W.E. Zandbergen, Physica C 158 (1989) 391.
[3] F. Abbattista, M. Vallino, D. Mazza, M.L. Borlera, C. Brisi, Mater. Chem. Phys. 20 (1988) 191.
[4] F. Abbattista, M. Vallino, D. Mazza, Mater. Chem. Phys. 20 (1989) 521.
[5] P.W. Anderson, Remarks at the Panel Discussion on d-wave Superconductor, J. Phys. Chem. Solids 54 (1993) 1457.
[6] Y.T. Zhu, P.S. Baldonado, E.J. Peterson, D.E. Peterson, F.M. Mueller, Powder diffraction 12 (1997) 242.
[7] Y.T. Zhu, E.J. Peterson, P.S. Baldonado, J.Y. Coulter, D.E. Peterson, F.M. Mueller, J. Phys. Chem. Solids 59 (1998) 1331.
[8] Y.T. Zhu, E.J. Peterson, P.S. Baldonado, J.Y. Coulter, D.E. Peterson, F.M. Mueller, Synthesis and crystal chemistry of the new compounds $GdBa_4Cu_3O_{8.5+\delta}$, and $DyBa_4Cu_3O_{8.5+\delta}$, J. Mater. Res. (in press).
[9] A.C. Lawson, R.B. Von Dreele, GSAS, Generalized Structural Analysis System, Document LAUR 86-748, Los Alamos National Laboratory, Los Alamos, New Mexico, 1993.
[10] Y.T. Zhu, P.S. Baldonado, E.J. Peterson, Y.S. Park, A. Manthiram, D.P. Butt, D.E. Peterson, F.M. Mueller, Variation of oxygen content and crystal chemistry of $YbBa_4Cu_3O_{8.5+\delta}$, Physica C 298 (1998) 29.
[11] J.A. Dean, Lange's Handbook of Chemistry, 4th ed., ch. 4, McGraw-Hill, New York, 1992, pp. 13–17.
[12] Y.T. Zhu, A. Manthiram, Role of bond-length mismatch in $L_{2-x}Ce_xCuO_4$ (L=lanthanide), Phys. Rev. B 49 (1994) 6293.
[13] Y.T. Zhu, A. Manthiram, A thermogravimetric study of the influence of internal stresses on oxygen variations in $L_{2-x}Ce_xCuO_4$, J. Solid State Chem. 114 (1995) 491.
[14] M.B. Maple, Y. Dalichaouch, J.M. Ferreira, R.R. Hake, B.W. Lee, J.J. Neumeier, M.S. Torikachvili, K.N. Yang, H. Zhou, R.P. Guertin, M.V. Kuric, Physica B 148 (1987) 155.
[15] J.T. Markert, Y. Dalichaouch, M.B. Maple, Rare earth and other substitions in high temperature superconductors, in: D.M. Ginsberg (Ed.), Physical Properties of High Temperature Superconductors I, ch. 6 World Scientific, Singapore, 1989, p. 265.